AIP | The Journal of Chemical Physics

Fullerene symmetry reduction and rotational level fine structure: The Buckyball isotopomer 12C59 13C

Tyle C. Reimer and William G. Harter

Citation: The Journal of Chemical Physics **106**, 1326 (1997); doi: 10.1063/1.473303
View online: http://dx.doi.org/10.1063/1.473303
View Table of Contents: http://scitation.aip.org/content/aip/journal/jcp/106/4?ver=pdfcov
Published by the AIP Publishing

Articles you may be interested in

Infrared spectroscopy of endohedral HD and D2 in C60
J. Chem. Phys. **135**, 114511 (2011); 10.1063/1.3637948

Coupled translation-rotation eigenstates of H 2 in C 60 and C 70 on the spectroscopically optimized interaction potential: Effects of cage anisotropy on the energy level structure and assignments
J. Chem. Phys. **130**, 224306 (2009); 10.1063/1.3152574

Rotational spectrum and carbon-13 hyperfine structure of the C 3 H , C 5 H , C 6 H , and C 7 H radicals
J. Chem. Phys. **122**, 174308 (2005); 10.1063/1.1867356

Molecular parameters for 12 C and 13 C -methanol isotopomers with O-16, 17, and 18
J. Chem. Phys. **112**, 212 (2000); 10.1063/1.480573

Rotational spectra, structure, and internal dynamics of Ar–H 2 S isotopomers
J. Chem. Phys. **106**, 5309 (1997); 10.1063/1.473066

This article is copyrighted as indicated in the article. Reuse of AIP content is subject to the terms at: http://scitation.aip.org/termsconditions. Downloaded to IP: 132.248.9.8
On: Mon, 22 Dec 2014 16:28:40

Fullerene symmetry reduction and rotational level fine structure: The Buckyball isotopomer $^{12}C_{59}$ ^{13}C

Tyle C. Reimer and William G. Harter
University of Arkansas, Fayetteville, Arkansas 72701

(Received 18 July 1996; accepted 14 October 1996)

Rotational level structure is investigated for a number of lower symmetry fullerene structures including the Buckyball isotopomer ^{13}C $^{12}C_{59}$, and it is compared to that of $^{12}C_{60}$ using quantum mechanical and semiclassical theory. Rotational spectra of ^{13}C $^{12}C_{59}$ differs markedly from that of icosahedrally symmetric Buckyball because the presence of a single additional neutron completely breaks its rotational symmetry from I_h for C_{60} down to a single C_s reflection plane for ^{13}C $^{12}C_{59}$. Nevertheless, most rotational energy levels remain surprisingly clustered and well ordered. Predictions are made for types of spectroscopic structure resulting from reduction of icosahedral symmetry to C_s, C_{2v}, C_{3v}, and C_{5v} such as might be encountered in intrahedrally doped XC_{59}. Semiclassical techniques help to label the spectra of molecules undergoing such extreme symmetry breaking and to explain why high J levels still maintain so much order and degeneracy under these conditions. These techniques may also be useful toward understanding the dynamics of hindered rotors in solution or solid fullerite, as well as in the interpretation of high resolution gas phase spectra of fullerene molecules or ions. © *1997 American Institute of Physics.* [S0021-9606(97)00504-7]

I. INTRODUCTION

With the introduction of less expensive production techniques[1,2] there has been a flurry of interest in the fullerenes which include a myriad of carbon cage structures, varying from the spherical Buckminsterfullerene (C_{60}) to elongated carbon ''bucky-tubes.'' Mass spectroscopy shows evidence of superfullerenes made of hundreds of carbon atoms,[3] and TEM reveals fullerenes nesting in a fashion similar to the layers of an onion.[4] As more of the nature of these fullerenes are unveiled it becomes apparent that the fullerenes comprise a new family of organic molecules, with many more varieties and symmetries than the planar hydrocarbons. Also, extensions of fullerene compounds such as the metallo-carbohedranes[5] or ''metcars'' (X_mC_{n-m}) can be viewed as an *intrahedral* doping or substitution of m of the n original carbons which represents a lowering of the icosahedral (I_h) symmetry of a pure C_n molecule to one of T_h symmetry.

The fullerenes may also be doped in an *endohedral* ($X@C_n$) manner by trapping the X-impurity inside the cage. Lanthanum and potassium have been endohedrally trapped during formation of C_{60} (see Ref. 6) and may play the role of nucleation site by helping a hexagonal carbon lattice become nonplanar. High energy injection methods have also been used to endohedrally dope Buckyball with helium atoms.[7,8] Finally, there is the possibility of *exohedral* doping or surface absorption on the exterior of the cages.[9]

The possible point symmetries of the various fullerene and ''metcar'' structures range from I_h (icosahedral-inversion symmetry used to be labeled Y_h), the highest point symmetry in 3-space, through a multitude of lower point symmetries including (most often) no symmetry at all. Many of these symmetries can be obtained by replacing carbon ^{12}C atoms by the next most abundant isotope ^{13}C. Indeed, a single ^{13}C in C_{60} reduces I_h symmetry to only bilateral reflection or C_s symmetry, and two or more ^{13}C isotopes for most steric placements leave the Buckyball cage with no symmetry at all. For Buckyball composed of both ^{12}C and ^{13}C atoms there are a vast number of substructures that can be formed each with their own inherent symmetries and probabilities of formation. For a fractional natural abundance of $p=0.011$ for ^{13}C, the probability $P(p,n)$ for a 60 carbon $^{13}C_n$ $^{12}C_{60-n}$ molecule composed of n ^{13}C atoms is given by the following:

$$P(p,n)=\frac{60!}{n!(60-n)!}\,p^n(1-p)^{60-n}=\begin{cases}0.52 & \text{for } n=0,\\ 0.34 & \text{for } n=1,\\ 0.11 & \text{for } n=2.\end{cases} \tag{1.1}$$

Of all the C_{60} isotopomers, only $^{12}C_{60}$ and $^{13}C_{60}$ have the high icosahedral symmetry. High symmetry molecules have levels with more degeneracy. (I-symmetry species A, $T1$, $T2$, G, and H have degeneracy 1, 3, 3, 4, and 5, respectively.) Also, high symmetry molecules exhibit a near-degeneracy known as spectral clustering or superfine structure[10–12] which for I-symmetry gives degeneracies of 12, 20, and 30. So, level structure of high symmetry rotors is sparse, and more so for higher symmetry.

Except for trivial mass rescaling, $^{12}C_{60}$ and $^{13}C_{60}$ have the same rotational and rovibrational Hamiltonians and spectra. However, since ^{12}C nuclei are spin-0 the Bose–Einstein exclusion principle excludes all but 1 in 60 of the $^{12}C_{60}$ rotational states. (Only A_g states are allowed. Roughly speaking, this is because all sixty rotational I-symmetry positions are truly indistinguishable.) The result is extremely sparse rotor levels, perhaps the most extreme rotor symmetry exclusion that has ever existed.[13]

On the other hand, since ^{13}C nuclei are spin-$\frac{1}{2}$ all the I-symmetry species for $^{13}C_{60}$ are allowed.[13] (Even one ^{13}C spin is enough to distinguish all I-rotational positions.) Now,

This article is copyrighted as indicated in the article. Reuse of AIP content is subject to the terms at: http://scitation.aip.org/termsconditions. Downloaded to IP: 132.248.9.8 On: Mon, 22 Dec 2014 16:28:40

$^{13}C_{60}$ superfine and hyperfine structure is much more complex since 60 spin-$\frac{1}{2}$ nuclei give rise to 2^{60} Pauli–Fermi–Dirac-allowed hyperfine states.[13] Nevertheless, for small hyperfine splitting, the $^{13}C_{60}$ rotational spectrum is still quite sparse because of the symmetry effects mentioned above.

One might expect that the low symmetry of $^{13}C_n\ ^{12}C_{60-n}$ isotopomers and most other doped fullerenes, might doom them to having inordinately complex rotor spectra. However, we shall show that spectra of $^{13}C\ ^{12}C_{59}$ (which has no rotational symmetry at all), is relatively simple and comprehensible, at least for the models considered below. Features of the rotational level structure for $^{13}C\ ^{12}C_{59}$ will be considered using semiclassical and quantum mechanical analysis. Such features are expected to appear in high resolution rotation-vibration spectra of a gas containing fullerenes produced without isotopic selection since $^{13}C\ ^{12}C_{59}$ has the highest natural abundance; 34% by Eq. (1.1). Similar features can be expected when the C_{60} fullerene has its symmetry broken other ways, and some of these will be discussed subsequently.

First, we show the method of describing lower symmetry rotational levels by considering a model rotational Hamiltonian of the $^{13}C\ ^{12}C_{59}$ rotor.

II. APPROXIMATING THE SEMIRIGID $^{13}C\ ^{12}C_{59}$ ROTATIONAL HAMILTONIAN

A symmetry analysis of the isotopomer $^{13}C\ ^{12}C_{59}$ shows that its icosahedral symmetry has been greatly reduced because the ^{13}C atom occupies a site with only a reflection plane for local symmetry. The purely rotational icosahedral symmetry I is reduced to the C_1 identity group, while the full icosahedral symmetry $I_h = I \otimes C_i$ is reduced to a group C_s of order two. This implies that many of the degeneracies due to the icosahedral symmetry split into C_s singlets when the molecule distorts due to rotation.

However, a rigid isotopomer $^{13}C\ ^{12}C_{59}$ has the same inertia tensor as a spherical shell with an imbedded point of neutron mass. This is a slightly prolate rigid *symmetric* top with an R_2-symmetric rotational Hamiltonian:

$$\mathbf{H}_{\mathrm{sym}} = BJ^2 + (A-B)J_z^2. \tag{2.1}$$

The rotational constant is $B = 0.0028\ \mathrm{cm}^{-1} = 84$ MHz for $^{12}C_{60}$. The longitudinal versus transverse rotational constant difference ($A - B = 3.6$ MHz) is due to the extra ^{13}C neutron. (There is tiny correction due to a tiny shift in the center of mass, however this will be ignored here since it is of the order of the uncertainty for the C_{60} bond lengths.)

In irreducible tensor notation $\mathbf{H}_{\mathrm{sym}}$ has the following form:

$$\mathbf{H}_{\mathrm{sym}} = \frac{A+2B}{3}\,\mathbf{T}_0^0 + \frac{2A-2B}{3}\,\mathbf{T}_0^2. \tag{2.2a}$$

The second rank angular momentum tensor operators are defined as follows:

$$\mathbf{T}_0^0 = J \bullet J = J_x^2 + J_y^2 + J_z^2,$$
$$\mathbf{T}_0^2 = -\tfrac{1}{2}J_x^2 - \tfrac{1}{2}J_y^2 + J_z^2. \tag{2.2b}$$

Tensor notation[14] facilitates matrix evaluation, rotational symmetry, and the semiclassical graphical analysis which follows. It also helps to simplify the description of centrifugal and coriolis distortion operators which can become unnecessarily complicated if written as polynomials. [Compare Eq. (2.3) below with Eq. (3.3) in the following section.]

Icosahedral symmetry requires that the simplest anisotropic distortion operator must have a specific sixth degree (or rank) tensor form given by Eq. (2.3) below. Here the chosen body z-axis of quantization is an icosahedral fivefold symmetry axis with the x- and z-axes lying in a C_s reflection plane:

$$\mathbf{H}_{\mathrm{icosa}} = t_{066}\left[\frac{\sqrt{11}}{5}\,\mathbf{T}_0^6 + \frac{\sqrt{7}}{5}\,(\mathbf{T}_5^6 + \mathbf{T}_{-5}^6)\right]. \tag{2.3}$$

The next highest allowed icosahedral operator is of tenth degree in J. The rotational level spectra of icosahedral operators have been discussed previously.[10–16] The evaluation of tensor molecular constants such as t_{066} is beyond the scope of this work since they require detailed and accurate *an*harmonic force field calculations. (The better known spherical top molecules such as C_8H_8 and SF_6 have cubic-octahedral symmetry, and they are well described using distortion operators of only fourth rank which are related in a relatively simple way to harmonic force constants.)

It is even more difficult to predict the values of vibrationally excited centrifugal-coriolis constants t_{a6-a6} ($a = 2,4$) for $^{12}C_{60}$. The scalar coriolis constants $B\zeta$ were predicted for the four dipole active modes.[17] These were approximately verified in low resolution Fourier transform infrared (FTIR) spectra.[18] A dynamical model by Weeks[19] has given values for pure vibrational splittings of $^{13}C\ ^{12}C_{59}$. Perhaps it can be extended to predict $^{13}C\ ^{12}C_{59}$ tensor fine structure splitting, as well. For now, the C_{60} tensor constants remain unknown.

Instead of guessing a value for constants like t_{066}, a range of values of the tensor contribution (2.3) will be explored. We consider the eigenlevels of the following model rotational Hamiltonian (2.4) which has continuously variable amounts of I_h and C_s symmetric parts (2.3) and (2.2), respectively:

$$\mathbf{H} = \mathbf{H}'_{\mathrm{sym}} + \mathbf{H}_{\mathrm{icosa}}. \tag{2.4}$$

However, it is necessary to take account of the relative orientation of the two tensor terms. From the geometry of the fullerene structure we find that the polar angle β_p subtending to the C^{13} site has the following value

$$\beta_p = \tan^{-1}\left(\frac{2-8F^-}{19}\right) = 0.350\,405\,41\ldots,$$

where

$$F^- = \frac{1-\sqrt{5}}{2}. \tag{2.5a}$$

The $\mathbf{H}'_{\mathrm{sym}}$ term is a rotated version of $\mathbf{H}_{\mathrm{sym}}$ using a body-frame rotation by Euler angles ($\beta_p = 0.35\ldots$, $\gamma_p = 0$) to align the effective prolate top axis with the ^{13}C site.

$$\mathbf{H}'_{\mathrm{sym}} = \mathbf{R}^{-1}(\cdot,\beta_p,\gamma_p)\mathbf{H}_{\mathrm{sym}}\mathbf{R}(\cdot,\beta_p,\gamma_p). \tag{2.5b}$$

This article is copyrighted as indicated in the article. Reuse of AIP content is subject to the terms at: http://scitation.aip.org/termsconditions. Downloaded to IP: 132.248.9.8
On: Mon, 22 Dec 2014 16:28:40

Rotational transformations are given as linear combinations of the irreducible tensors with Wigner D-function coefficients as described below. It is computationally simpler to align the second rank tensors in $\mathbf{H}_{\mathrm{sym}}$ with the sixth rank ones in $\mathbf{H}_{\mathrm{icosa}}$ rather than the other way around, but either way should yield the same results.

Higher rank semirigid axial or symmetric top distortion operators such as $\mathbf{T}_0^0$, $\mathbf{T}_0^4$, and additional $\mathbf{T}_0^6$ are ignored in this model since they do not appear to qualitatively change the outcome. The $\mathbf{H}_{\mathrm{sym}}$ and $\mathbf{H}_{\mathrm{icosa}}$ terms vary like $|J|^2$ or $|J|^6$, respectively, and so the sixth rank tensor terms would start to dominate for higher J. As mentioned previously, tenth and higher rank icosahedral tensors are possible, but we are not considering those effects here for lack of constant values. Asymmetric distortion operators such as $\mathbf{T}_2^4$ or $\mathbf{T}_4^4$ might be important for heavy dopants but probably not for just one neutron. For lower J values and up to some critical J the symmetric top term (2.2a) would presumably be most influential, followed then by the sixth rank distortion term (2.3) which is allowed in the original isotopically pure C_{60} molecule.

In the usual angular momentum basis, the quantum-mechanical Hamiltonian has the following representation, where Wigner D-matrices are used to rotate the axial or symmetric top irreducible tensor parts.

$$H_{KK'}=B|J|^2+t_{066}\langle J\|6\|J\rangle\left[\frac{\sqrt{11}}{5}\,C^{6JJ}_{0KK}\delta_{KK'}+\frac{\sqrt{7}}{5}\times(C^{6JJ}_{5KK+5}\delta_{K+5,K'}+C^{6JJ}_{-5KK-5}\delta_{K-5,K'})\right]+\frac{2A-2B}{3}\times\langle J\|2\|J\rangle\sum_{n=-2}^{2}D^2_{0n}(\cdot,\beta,\gamma)C^{2JJ}_{nKK+n}\delta_{K+n,K'}. \quad (2.6)$$

To aid in viewing and analysis, the zero rank term is set to unity and a parameter τ is introduced which will contain all coefficients and reduced matrix elements. The higher ranked terms are then rescaled to $\frac{2}{10}$ of the scalar term:

$$H_{KK'}=\delta_{KK'}+\frac{2}{10}\left\{\tau\sum_{n=-2}^{2}D^2_{0n}(\cdot,\beta,\gamma)C^{2JJ}_{nKK+n}\delta_{K+n,K'}+(1-\tau)\left[\frac{\sqrt{11}}{5}\,C^{6JJ}_{0KK}\delta_{KK'}+\frac{\sqrt{7}}{5}\,(C^{6JJ}_{5KK+5}\delta_{K+5,K'}+C^{6JJ}_{-5KK-5}\delta_{K-5,K'})\right]\right\}. \quad (2.7)$$

Note that τ represents the relative amounts of second rank terms with respect to the sixth rank terms and would be J-dependent for fixed molecular constants t_{066}, B, and A. The spectra for XC_{59} single site doping will differ from that of $^{13}C\ ^{12}C_{59}$ by the value of A, B, and t_{066} and hence of τ. Furthermore, certain types of doping at sites with other than C_s local symmetry may be treated as above with an appropriate choice of Euler angles (β_p,γ_p) and will be analyzed subsequently.

III. ROTATIONAL ENERGY SURFACE VIEWS

In order to view the eigensolutions of model Hamiltonian (2.4) in a semiclassical manner, a rotational energy (RE) surface is constructed using the asymptotic expectation values of the tensor operators $\mathbf{T}^{\mathrm{r}}_{\mathrm{q}}$,

$$T^r_q\rightarrow D^r_{0q}(\cdot,-\beta,-\gamma)|J|^r=C^r_q(\theta,\phi)|J|^r. \quad (3.1)$$

The asymptotic values involve Wigner D-functions D^r_{0q}, and multipole functions C^r_q which are closely related to spherical harmonics Y^r_q. The polar (θ) and azimuthal (ϕ) angles locate the classical angular momentum relative to the body frame. The polar angles are related to the Euler angles (β,γ) by

$$\theta=-\beta,\quad \phi=-\gamma, \quad (3.2)$$

and are used to plot the trajectories associated with the evolution of classical angular momentum vectors for fixed magnitude $|J|$ and constant energy.[11] The classical Hamiltonian derived from (2.7) has the following polynomial form upon replacement of each rank r tensor operator $\mathbf{T}^{\mathrm{r}}_{\mathrm{q}}$ with a corresponding rth degree multipole function C^r_q.

$$H=1+\tfrac{2}{10}\tau\{\tfrac{3}{4}\sin^2(\beta_p)\sin^2(\theta)\cos(2\phi)+\tfrac{3}{4}\sin(2\beta_p)\sin(2\theta)\cos(\phi)+\tfrac{1}{4}[3\cos^2(\beta_p)-1][3\cos^2(\theta)-1]\}+\tfrac{2}{10}(1-\tau)\times\{\tfrac{1}{16}[231\cos^6(\theta)-315\cos^4(\theta)+105\cos^2(\theta)-5-42\sin^5(\theta)\cos(\phi)(5-20\phi^2+16\phi^4)]\}. \quad (3.3)$$

As in the case of (2.7) the τ coefficients depend upon other coefficients and are scaled to $\frac{2}{10}$ of the scalar term, and $\beta_p=0.35...$ is given by (2.5a).

IV. LEVEL STRUCTURE AND ROTATIONAL ENERGY SURFACE TRAJECTORIES

The RE surfaces for $J=50$ are plotted along the top of Fig. 1 for six values of $\tau=[0,\frac{1}{5},\frac{2}{5},\frac{3}{5},\frac{4}{5},1]$ giving a variety of classical RE surface shapes. Below each of them in Fig. 1 are the exact energy levels which are obtained by diagonalizing the tensor $2J+1$ by $2J+1$ Hamiltonian matrix given by Eq. (2.7) for $J=50$ while varying τ from $\tau=0$ to $\tau=1$. The classical J trajectories are topography lines (constant energy) near ''quantizing'' classical levels corresponding to certain parts of the quantum energy level spectra indicated by arrows in Fig. 1 pointing directly below each shape. (The paths drawn in the figures are generic, i.e., not precisely the quantizing paths for $J=50$, but they have essentially the correct form in each case.)

The RE surface plots may be viewed as rotational phase-

This article is copyrighted as indicated in the article. Reuse of AIP content is subject to the terms at: http://scitation.aip.org/termsconditions. Downloaded to IP: 132.248.9.8 On: Mon, 22 Dec 2014 16:28:40

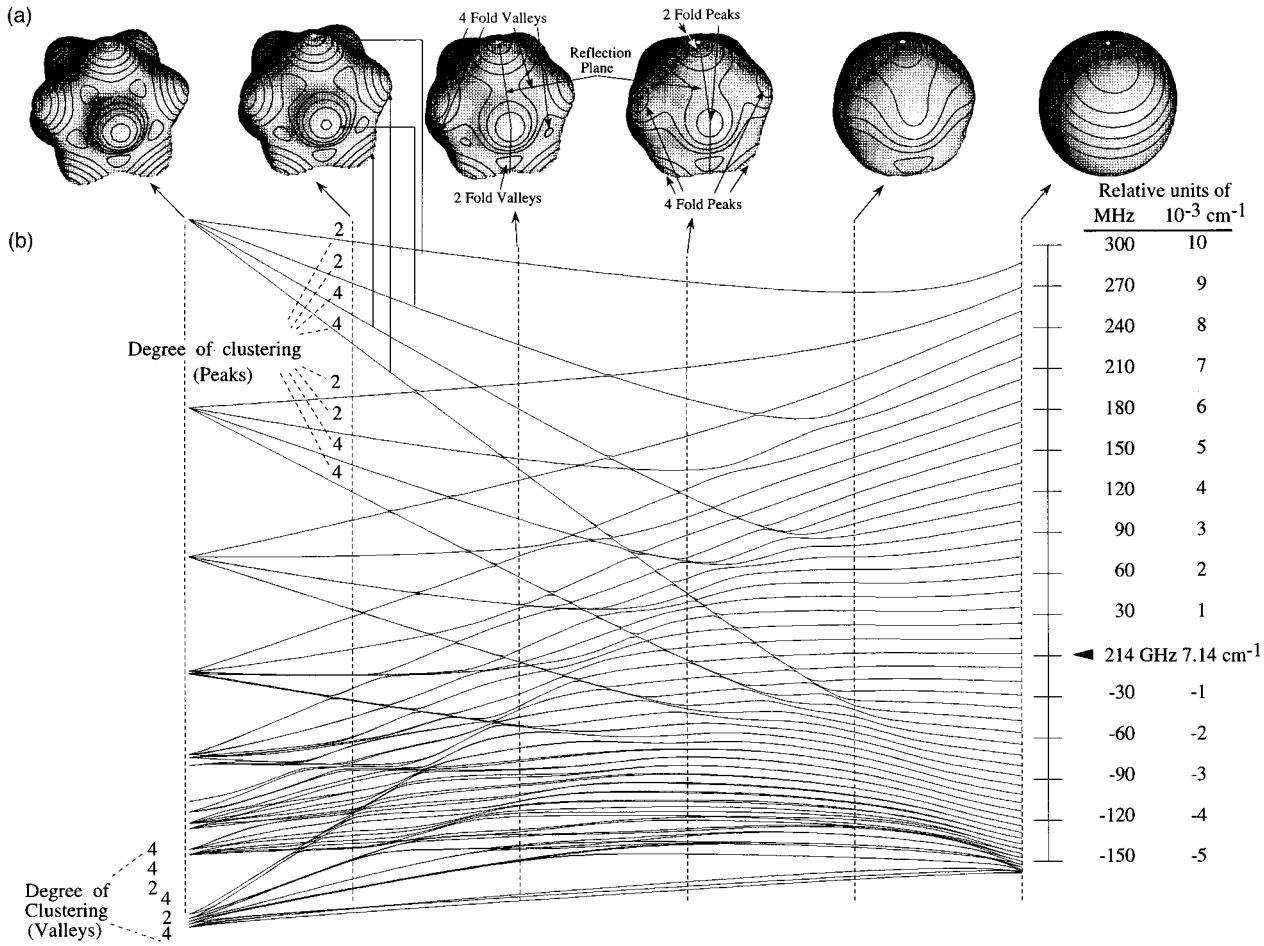

FIG. 1. Rotational energy surfaces and ($J=50$) levels for Cs symmetry breaking. (a) Rotational energy surfaces varying from pure semirigid icosahedral (left) to pure symmetric top (right) molecules for $\tau=0,\frac{1}{5},..,1$. (b) Quantum mechanical energy levels for $|J|=50$ varied from pure semirigid icosahedral molecule (left) to purely rigid symmetric top perturbation. The energy scale on the right applies to rigid $^{13}C\ ^{12}C_{59}$ prolate top levels.

space portraits. Each quantizing phase path corresponds to an eigenfunction or set of eigenfunctions belonging to a given level or cluster of levels. Multiply congruent paths belong to a multiplet of levels, which would have degenerate classical energies, but are split slightly by tunneling in the quantum system. Tunneling would occur, for example, between equivalent paths in different regions having the same local symmetry and energy. Tunneling is smallest for paths that are localized and well separated by intervening valleys. Examples of different path and level structures are now given for the different cases of RE surfaces belonging to different values of τ.

A. Pure icosahedral (I_h) symmetry ($\tau=0$)

The extreme left of Fig. 1 is the limiting case for $\tau\rightarrow 0$ and would correspond more nearly to the spectrum one expects for high J where high-ranking coriolis and centrifugal effects are dominant. The limit $\tau=0$ belongs to the pure icosahedrally symmetric energy levels and RE surface.[10]

Consider the (I_h) symmetric RE surface on the left hand ($\tau=0$) side of Fig. 1. The 12 peaks contain higher energy pentagonal trajectories that have C_5 local symmetry and correspond to a 12-fold nearly degenerate clusters. Similarly, the 20 equivalent valleys have C_3 symmetry and correspond to a 20-fold nearly degenerate clusters at the extreme lower left-hand side of Fig. 1. There is only room for one C_3 cluster because its eigenfunctions must occupy a smaller percentage of the available rotational phase-space to avoid the separatrix. Also the C_3 cluster is split more than the C_5 clusters because the tunneling across the separatrix is greater.

Dividing these well-defined C_5 and C_3 regions of nonzero curvature is the separatrix region which contains points of inflection or saddle points. This region contains the boundary between the fivefold and threefold symmetry regions and corresponds to delocalized and unclustered states that are very sensitive to changes in the parameter τ. They would also be states most susceptible to other perturbations of the Hamiltonian.

In contrast, for the high and low energy values there is very tight level clustering for states that are much more localized and less sensitive to perturbations. This is typical of the rotational and rovibrational spectra obtained for highly symmetric molecules. This clustering is the rotational symmetry analog to the band structure exhibited in solids with translational symmetries. The high energy clusters contain

This article is copyrighted as indicated in the article. Reuse of AIP content is subject to the terms at: http://scitation.aip.org/termsconditions. Downloaded to IP: 132.248.9.8
On: Mon, 22 Dec 2014 16:28:40

groups of 12 nearly degenerate levels, many of which are exactly degenerate I multiplets. The low energy clusters contain groups of 20 levels. Within these clusters of 12 and 20 nearly degenerate levels there are sublevels with standard symmetry degeneracies of the order 1, 3, 3, 4, or 5, corresponding to the dimension of icosahedral symmetry species A, T_1, T_3, G, and H, respectively. Several unclustered I multiplets separate the high and low energy bands of clusters in the separatrix region. I-cluster superfine structure is described in detail in Refs. 10 and 12.

The bands of energy level structures can be associated with paths on the leftmost RE surface directly above. White dots at the tops of the RE surfaces show the body's azimuthal axis chosen to be a fivefold rotational axis. The visible portions of 12 rotationally equivalent peaks containing the C_5 symmetric trajectories of the classical angular momentum vectors are indicated by the dark loops or level curves. The trajectories for the single 20-fold C_3 symmetric cluster can be seen in the low energy triangular valleys.

On each surface in Fig. 1 there are six equally spaced level curves which correspond to states of equally spaced energy. These trajectories may be envisioned as expectation trajectories for the angular momentum vectors in coherent states composed of the quantum-mechanical states belonging to the corresponding clusters. The six levels are enough to approximate the different kinds of quantizing trajectories for $J=50$, though of course they do not show their exact positions. (One set of equi-energy quantizing trajectories exists for each level cluster.)

B. Pure symmetric top R_2 symmetry ($\tau=1$)

For low angular momentum, (or equivalently $\tau\rightarrow 1$) the second order tensor terms in Eq. (2.4) play the dominant role and in the extreme case ($\tau=1$) the pure symmetric top Hamiltonian is obtained. Along the right-hand edge of Fig. 1(b), the energy levels are plotted for a rotating symmetric top with the same $J=50$. The energy-frequency units are calculated using Eq. (2.1), and the level manifold center of gravity is taken as an origin.

All but one of the rigid symmetric top levels occur in twofold clusters comprised of rotationally degenerate doublets labeled by symmetric top R_2 symmetry species ($\Pi,\Delta,\Phi,...$). This is one of the rare cases where each level cluster belongs to a single symmetry species or *irreducible* representation of the global molecular symmetry. In general, clusters belong to locally *induced* representations of the global symmetry.[11]

The lowest eigenvalue corresponds to the only singlet and is labeled as the Σ species. In the accompanying RE surface drawn above the levels, two equivalent peaks are inscribed with six ''generic'' examples of the 51 quantizing trajectories belonging to $J=50$ and $K=0$, ± 1, $\pm 2,...,\pm 50$. The waist of the surface contains the trajectory of singlet ($K=0$) state and would be referred to as the separatrix if it actually separated differing types of clusters. A more comprehensive symmetry analysis of the rotational spectra of these symmetric molecules can be found in Ref. 11.

C. Intermediate C_s symmetry ($0<\tau<1$)

The values of τ that lie between 0 and 1 will most likely have physical meaning for $^{12}C_{59}$ ^{13}C. As viewed from right to left, the successive RE surfaces in Fig. 1(a) show rotational deformation that the symmetric top angular momentum trajectories would undergo as $|J|$ increases and more of the molecule's underlying icosahedral structure comes into play through centrifugal distortion. The maxima of symmetric top RE surface splits into three pairs of maxima, and five minima. One pair of maxima lie in the plane of C_s reflection symmetry and the other two pair straddle this plane. The pentad of minima are joined by another pentad of minima evolving from the separatrix region. The same process occurs on the other side of the RE surface and finally leads to the 20 equidistant C_3 symmetric minima and the 12 C_5 symmetric maxima of the pure icosahedral surface.

The mixed RE surfaces provide information about the quantum-mechanical spectra for ^{13}C $^{12}C_{59}$. The RE extrema found on the reflection plane appear in equivalent pairs, while those off plane fall into groups of four. The radial placement on the surface (energy is altitude or radius) gives the ordering of these two- and fourfold clusters that correspond to the pure icosahedral 12 and 20-fold clusters. The 12-fold clusters split into subclusters of order 2, 2, 4, and 4 and the 20-fold clusters break into subclusters of order 4, 4, 2, 4, 2, and 4. This ordering is visible near the separatrix region in the RE surfaces as τ increases. The clusters nearest the separatrix lose their icosahedral clustering characteristics sooner than the more isolated extreme energy clusters. Those energy levels not belonging to any well-defined cluster are perturbed almost immediately upon making τ nonzero, and this is evident by the prominent mixing of levels. Similarly, as τ becomes less than 1, the symmetric top Σ singlet and low lying doublets are first to mix.

The symmetry labeling of the twofold and fourfold subclusters can be determined by relating the local symmetry of the corresponding trajectories to the global symmetry of the RE surface. Noting that the RE surface must be invariant to angular momentum inversion or time reversal, the global symmetry is $C_{2h}=C_s\times C_i$. The twofold trajectories lie on the plane of symmetry and therefore the twofold subclusters correspond to A_+ and A_- C_s symmetry species induced to C_{2h}, namely $A_+\uparrow C_{2h}=0_{2g}\oplus 1_{2u}$ and $A_-\uparrow C_{2h}=0_{2u}\oplus 1_{2g}$. The 4-fold trajectories have only trivial local symmetry and therefore the fourfold subclusters are induced by the trivial A-C_1 symmetry species induced to C_{2h}, or $A\uparrow C_{2h}=0_{2g}\oplus 1_{2g}\oplus 0_{2u}\oplus 1_{2u}$. This implies that in all subclusters no *true* rotational degeneracies exist, only singly degenerate lines will occur for $0<\tau<1$. However, nearly degenerate twofold and fourfold clusters are prevalent.

As in the $\tau=0$ and 1 extremes, clusters of a given type appear to emerge from the separatrix in an exponential manner. The number of contiguous clusters that appear is determined by the amount of phase-space available to those trajectories. An approximation using angular momentum cone geometry[11] can be used to estimate the number of clusters allowed before mixing into the separatrix region. This in-

This article is copyrighted as indicated in the article. Reuse of AIP content is subject to the terms at: http://scitation.aip.org/termsconditions. Downloaded to IP: 132.248.9.8
On: Mon, 22 Dec 2014 16:28:40

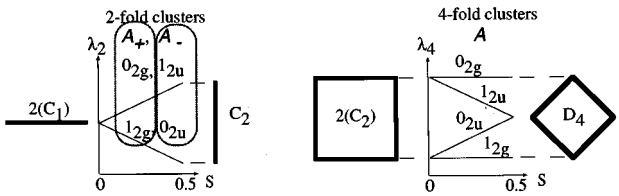

FIG. 2. Superfine structure of twofold and fourfold subclusters for C_s symmetry breaking.

volves finding a minimum or cutoff value K_{cutoff} for the azimuthal quantum number. Clusters can then be labeled by azimuthal quantum number $K=50,\ldots,K_{\text{cutoff}}$. Critical angles θ_{critical} separating dissimilar regions on the RE surface are then used to find the cutoffs. θ_{critical} is the angle between a local symmetry axis of quantization or classically stable fixed point and the nearest (unstable) separatrix point. From this angle we derive the cutoff value

$$K_{\text{cutoff}}=\sqrt{J(J+1)}\,\cos(\theta_{\text{critical}}). \tag{4.1}$$

In the symmetric top case ($\tau=1$) an angle of 90° separates the two-fold maxima from the separatrix giving a cutoff of $K_{\text{cutoff}}=0$ for all J. The critical angle in the pure icosahedral case ($\tau=0$) for the 12-fold clusters is $\theta_{\text{critical}}=26.6°$ giving a ($J=50$) cutoff of $K_{\text{cutoff}}=45$, which is observed in Fig. 1. Similarly, the 20-fold critical angle of 10.8° gives a ($J=50$) cutoff of $K_{\text{cutoff}}=50$ allowing only the lone 20-fold cluster observed at the bottom of Fig. 1. Cutoffs for the broken symmetry cases may be approximated in a similar fashion once the critical angles between extremal points and separatrices are given. The clusters that dominate in the RE surfaces have lower cutoff points and persist through the widest range of τ values. The highest twofold clusters and lowest twofold and fourfold clusters span the majority of τ values.

D. Nuclear spin weights

With only a single ^{13}C there is no permutation symmetry considerations or exclusion of symmetry species. All species have the same weight: there are two spin-$\frac{1}{2}$ states. The examples below depend upon the dopant structure and may not be so simple.

V. C_s CLUSTER SUPERFINE LEVEL STRUCTURE

The superfine structure of the clusters determines the intrasubcluster level spacing. Splitting of the 2-fold clusters arises from tunneling between two equivalent C_s symmetric regions on the RE surface which has C_{2h} symmetry. Each pair of C_s symmetric regions would have a tunneling amplitude S corresponding to their locations along the plane of symmetry. The twofold tunneling Hamiltonian then has the form,

$$[H_{\text{2-fold}}]=\begin{pmatrix} H & S \\ S & H \end{pmatrix}, \tag{5.1}$$

with eigenvalues $\{\lambda_{\text{2-fold}}\}=H\pm S$. Figure 2(a) illustrates the

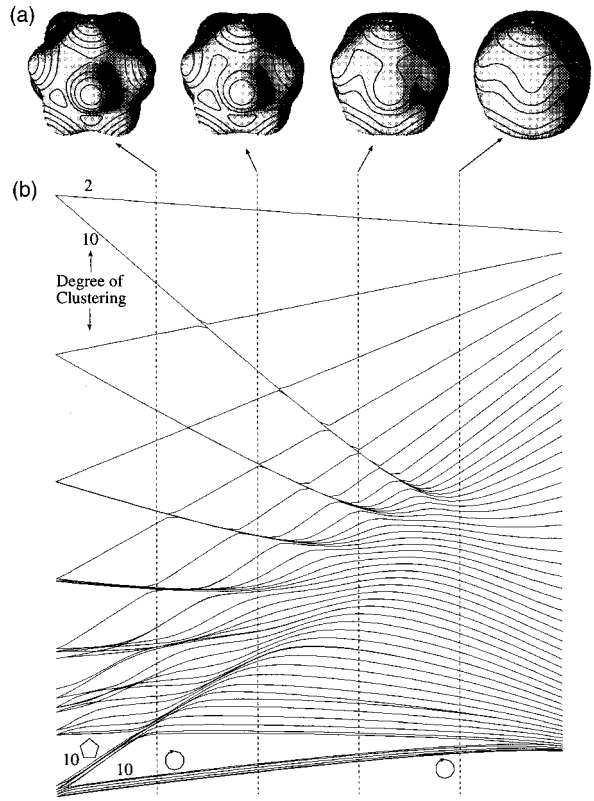

FIG. 3. Rotational energy surfaces and ($J=50$) levels for D_5-C_{5v} symmetry breaking. (a) Rotational energy surfaces varying from nearly icosahedral symmetry ($\tau=\frac{1}{5}$ on left) to nearly pure symmetric top ($\tau=\frac{4}{5}$ on right). (b) Quantum mechanical energy levels for $|J|=50$ varied from pure semirigid icosahedral molecule ($\tau=0$ on left) to pure symmetric top structure ($\tau=1$ on right) with dopant perturbation symmetry axis on a C_{5v} site.

A_+ and A_-. Twofold clusters labeled by C_{2h} symmetry species for $S\in[0,0.5]$. Note that the uppermost twofold peak of Fig. 1(a) is situated nearest the $\mathbf{H}_{\text{sym}}$ deformation and being more isolated would have less splitting than clusters arising from the remaining C_s regions. Also as $\tau\to 1$, the twofold trajectories become more isolated, S goes to zero and true twofold degeneracies are recovered for the symmetric top ($\tau=1$).

The intracluster level spacing for the fourfold subclusters can be determined in a similar manner. Tunneling occurs between a set of four equivalent regions on the RE surface, and each set would have tunneling amplitudes determined by their relative locations on the RE surface. This may be modeled by varying the relative amount of nearest-neighbor ($1-S$) and next-nearest-neighbor (S) tunneling amplitudes for $S\in[0,0.5]$ and setting the furthest-neighbor tunneling amplitude to zero. This fourfold tunneling Hamiltonian would have the form

$$[H_{\text{4-fold}}]=\begin{pmatrix} H & (1-S) & S & 0 \\ (1-S) & H & 0 & S \\ S & 0 & H & (1-S) \\ 0 & S & (1-S) & H \end{pmatrix}. \tag{5.2}$$

The eigenvalues are $\{\lambda_{\text{4-fold}}\}=H\pm 1,\ H\pm(1-S)$. Fig. 2(b) illustrates fourfold level spacing labeled by C_{2h} symmetry

This article is copyrighted as indicated in the article. Reuse of AIP content is subject to the terms at: http://scitation.aip.org/termsconditions. Downloaded to IP: 132.248.9.8
On: Mon, 22 Dec 2014 16:28:40

TABLE I. Correlation table relating C_5 species to D_5 species.

$D_5 \leftrightarrow C_5$	0_5	1_5	2_5	3_5	4_5
A_1	1	·	·	·	·
A_2	1	·	·	·	·
E_1	·	1	·	·	1
E_2	·	·	1	1	·

species for $S \in [0,0.5]$. $S=0$ gives two pair of widely spaced doublets of two independent twofold systems $\{2(C_2)\}$. The $S=0.5$ case corresponds to a D_4 like system with equal nearest-neighbor and next-nearest-neighbor tunneling amplitudes. For the values $0<S<0.5$, the fourfold level structure contains the species of the aforementioned C_{2h} regular representation. The level patterns for the extreme values of S can be related to the vertical spacing of the vertices of a square on edge ($S=0$) and on the point ($S=0.5$). For ($<S<0.5$) the fourfold clusters and can be related to the vertices of a square tilted between the aforementioned extremes.

VI. D_5-C_{5v} CLUSTER SUPERFINE LEVEL STRUCTURE

An analysis similar to that the one above is given here for symmetry breaking and superfine level structure in the case where doping lowers the global molecular point symmetry to C_{5v} and the rotational symmetry to D_5. The two are worth comparing since C_v is practically the lowest symmetry to which one can break an I_h structure while D_5 is the highest symmetry breaking that can be had with a dopant at a single C_{60} site.

RE surfaces for four intermediate value of $\tau=\frac{1}{5},\frac{2}{5},\frac{3}{5},\frac{4}{5}$ are drawn at the top of Fig. 3. The extreme values of τ ($\tau=0$ and $\tau=1$) correspond to RE surfaces identical to those of the same values in Fig. 1 and are omitted from all following illustrations. The original 12 equivalent icosahedral peaks are now split into 2 equivalent peaks that are of C_5 local symmetry and 10 equivalent peaks having C_s local symmetry. On the low end, the 20 equivalent valleys are perturbed into two sets of 10 equivalent valleys having C_s local symmetry. As τ goes from 0 to 1, less phase-space is available for the tenfold valleys and the level curves that they contain evolve into twofold C_5 symmetric trajectories.

In the lower portion of Fig. 3, quantum-mechanical eigenvalues for $J=50$ are plotted. The degree of clustering is labeled at the left-hand side. For small τ, each of the icosahedral high energy clusters contain corresponding twofold and tenfold subclusters as predicted above. As τ increases the tenfold clusters are seen to ''mix'' into twofold clusters. In the low energy region, the two tenfold subclusters corresponding to the icosahedral 20-fold clusters can be seen undergoing a similar evolution. The uppermost twofold and lowermost tenfold subclusters persist for nearly the entire range of τ values.

The superfine structure of the twofold clusters can be obtained by correlating the K_5 clusters with the global D_5 symmetry. The C_5 group is correlated to D_5 in Table I. The uppermost twofold cluster corresponds to an 0_5 cluster which from the 0_5 column of Table I. contains A_1 and A_2 species. The next lowest, a 4_5 twofold cluster, contains an E_1 doublet, the 3_5 an E_2 doublet, the 2_5 an E_2 doublet and the 1_5 doublet contains an E_1 doublet. The pattern then would cycle until it reaches the separatrix region. As τ increases the splitting between the 0_5 singlets goes to zero and all subclusters become symmetric top doublets except for one lone A_1 singlet that becomes an $R_2\Sigma$ species.

The superfine structure of the tenfold clusters can be approximated by using the tenfold Hamiltonian representation given below:

$$\mathbf{H}_{10\text{-fold}}=\begin{pmatrix} H & 1-S & \cdot & \cdot & 1-S & S & \cdot & \cdot & \cdot & S \\ 1-S & H & 1-S & \cdot & \cdot & S & S & \cdot & \cdot & \cdot \\ \cdot & 1-S & H & 1-S & \cdot & \cdot & S & S & \cdot & \cdot \\ \cdot & \cdot & 1-S & H & 1-S & \cdot & \cdot & S & S & \cdot \\ 1-S & \cdot & \cdot & 1-S & H & \cdot & \cdot & \cdot & S & S \\ S & S & \cdot & \cdot & \cdot & H & 1-S & \cdot & \cdot & 1-S \\ \cdot & S & S & \cdot & \cdot & 1-S & H & 1-S & \cdot & \cdot \\ \cdot & \cdot & S & S & \cdot & \cdot & 1-S & H & 1-S & \cdot \\ \cdot & \cdot & \cdot & S & S & \cdot & \cdot & 1-S & H & 1-S \\ S & \cdot & \cdot & \cdot & S & 1-S & \cdot & \cdot & 1-S & H \end{pmatrix}. \tag{6.1}$$

The cluster contains the species of the D_5 regular representation. In (6.1) the tunneling parameters are varied from pure pentagonal tunneling ($S=0$) to pure tunneling across the twofold axes ($S=1$). Figure 4 illustrates the various clustering found in Fig. 3(b). The lowermost tenfold cluster corresponds to S values close to 1 as would be expected from the collarlike arrangement of the low-lying tenfold congruent valleys in the RE surfaces of Fig. 3. The higher low energy tenfold cluster corresponds S values closer to zero corresponding to the tunneling to found in two independent pen-

This article is copyrighted as indicated in the article. Reuse of AIP content is subject to the terms at: http://scitation.aip.org/termsconditions. Downloaded to IP: 132.248.9.8 On: Mon, 22 Dec 2014 16:28:40

tagonal potentials. The tenfold high energy clusters have tunneling parameters S closer to a half and are characterized by singlet species separated by one or two doublet species.

VII. C_2 CLUSTER SUPERFINE LEVEL STRUCTURE

The effect of structural symmetry breaking on a C_2 axis is similar to that of the C_s symmetry breaking of Sec. V, with one difference being the presence of only 4-fold degenerate clusters. The overall pure rotational symmetry is D_2 which is isomorphic to $C_2 \otimes C_1$. Figure 5 illustrates the quantum-mechanical rotational energy levels with their associated RE surfaces.

The $\tau=0$ clusters all break up into three fourfold subclusters as τ becomes nonzero. Again these fourfold subclusters contain only rotational singlets until τ goes to 1. The two fourfold valleys situated near the waist of the RE surfaces are affected the least by the symmetric top perturbation and corresponding subclusters remain close to each other for small values of τ. Another interesting feature is the separation of the subclusters originating from the same 12-fold cluster. Since the symmetric top perturbation is aligned with the golden rectangles underlying the icosahedral structure the splitting would be related to the golden mean. The square of the radii of gyration for each type of fourfold site to the axis of rotation follows the proportionality $1{:}1+F^+{:}2+F^+$. Therefore, the ratio between the high energy fourfold centroids approach $1{:}F^+$. This is indeed the case for a great deal of the smaller τ values, and could prove to be an important feature in the description of rotational spectra of fullerene molecules having C_2-type doping.

VIII. C_3 CLUSTER SUPERFINE LEVEL STRUCTURE

Structural symmetry breaking due to a dopant at on a C_3 rotation axis of C_{60} is different from the other possibilities in that practically all the clusters have sixfold near degeneracy. The icosahedral-trigonal $(I-C_3)$ rotational energy surfaces and $J=50$ rotational level spectrum are shown in Fig. 6. for the same range of symmetry-breaking parameter τ as in the preceding figures which dealt with $I-C_5$ and $I-C_2$ symmetry reduction.

In the left central portion of Fig. 6 it can be seen that two sixfold near-degenerate clusters split away from each of the icosahedral level clusters which had 12-fold near degeneracy. This may be understood by examining the evolution of the twelve RE surface peaks as τ becomes nonzero in the upper left-hand part of the figure.

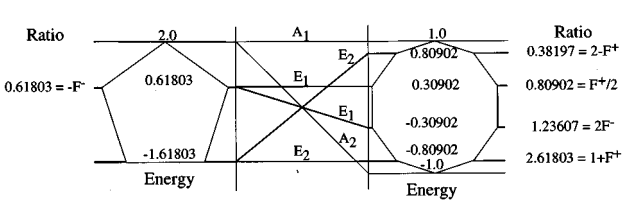

FIG. 4. Superfine structure of the tenfold subclusters for D_5-C_{5v} symmetry breaking.

The upper half of the RE surfaces for $\tau=\frac{1}{5}$, $\frac{2}{5}$, and $\frac{3}{5}$ have three peaks arranged in an equilateral triangle around the C_3 axis. On the opposite end of this axis the three inversion images of these peaks lie out of sight in the figures. Together these six equivalent peaks support quantizing trajectories for the upper sixfold near-degenerate clusters in each splitting. Near the C_3 axial equator there is another set of six equivalent peaks that are lower in energy and which account for the lower sixfold near-degenerate clusters in each splitting.

The 20-fold near-degenerate cluster at the extreme lower left-hand side of Fig. 6 undergoes a different sort of splitting into three sixfold near-degenerate clusters and a lone high-energy doublet. The doublet is associated with the two triangular encircling valley trajectories closest to either end of the C_3 axis. As τ approaches the symmetric top limit $(\tau=1)$ this doublet approaches the highest $(K=J=50)$ level in the symmetric top ladder. Its level trajectory can be seen rising diagonally from left to right in the figure.

One of the sixfold near-degenerate clusters is higher than the other two which tend to stick together until the symmetry breaking parameter exceeds about $\frac{2}{5}$. The higher cluster is associated with the three pairs of valley trajectories nearest

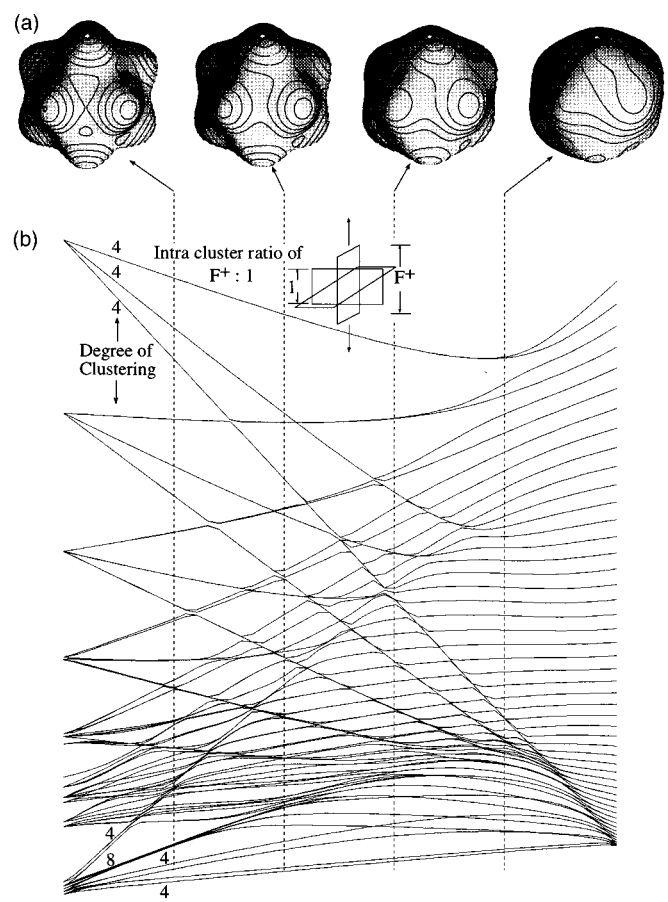

FIG. 5. Rotational energy surfaces and $(J=50)$ levels for $C_{2h}-C_{2v}$ symmetry breaking. (a) Rotational energy surfaces varying from nearly icosahedral symmetry ($\tau=\frac{1}{5}$ on left) to nearly pure symmetric top ($\tau=\frac{4}{5}$ on right). (b) Quantum mechanical energy levels for $|J|=50$ varied from pure semirigid icosahedral molecule ($\tau=0$ on left) to pure symmetric top structure ($\tau=1$ on right) with dopant perturbation symmetry axis on a C_{2v} site.

This article is copyrighted as indicated in the article. Reuse of AIP content is subject to the terms at: http://scitation.aip.org/termsconditions. Downloaded to IP: 132.248.9.8
On: Mon, 22 Dec 2014 16:28:40

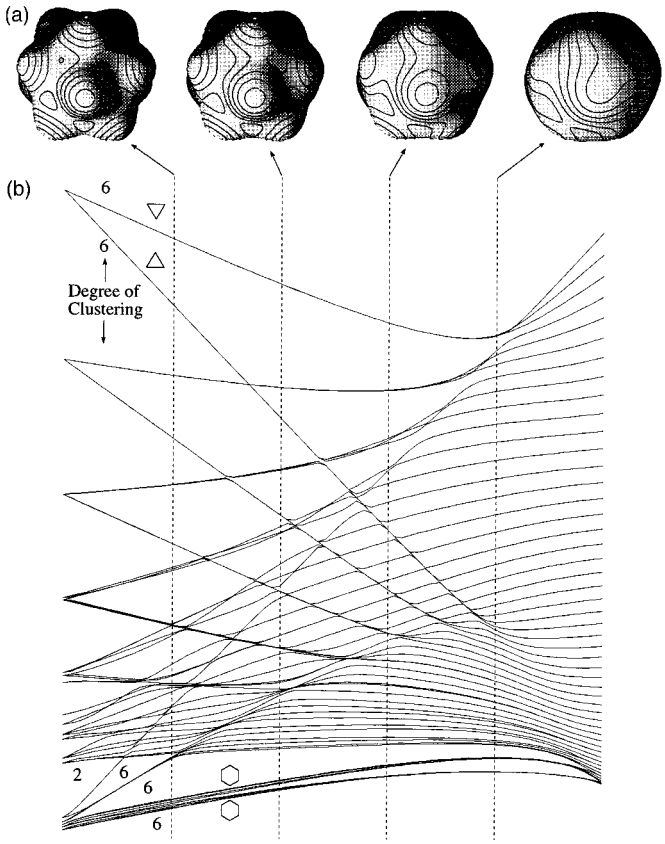

FIG. 6. Rotational energy surfaces and ($J=50$) levels for $D_{3d}-C_{3v}$ symmetry braking. (a) Rotational energy surfaces varying from nearly icosahedral symmetry ($\tau=\frac{1}{5}$ on left) to nearly pure symmetric top ($\tau=\frac{4}{5}$ on right). (b) Quantum mechanical energy levels for $|J|=50$ varied from pure semirigid icosahedral molecule ($\tau=0$ on left) to pure symmetric top structure ($\tau=1$ on right) with dopant perturbation symmetry axis on a C_{3v} site.

to the C_3 axis. They are in the neighborhoods of the three tiny loops visible on the ($\tau=\frac{1}{5}$) surface in Fig. 6. These tiny loops are about to disappear, and they have fallen off the slope of the ($\tau=\frac{2}{5}$) surface and all higher τ surfaces. Hence, the corresponding cluster is undergoing avoided crossing splitting just above $\tau=\frac{1}{5}$ though it leaves a 'cluster scar' in the level plot for higher τ values.

The other two lower energy sixfold near-degenerate clusters belong to a set of twelve equivalent paths located around the equator of the RE surface. Actually, they are six pairs of triangular loops with points facing each other across equatorial saddles. The tunneling across these saddles determines the splitting of the 12-fold cluster into its sixfold components which becomes significant for $\tau>\frac{2}{5}$ [see Fig. 7(a)].

The superfine structure within each of the two lower-energy sixfold clusters has the standard cyclic band structure.[14] For only nearest-neighbor azimuthal tunneling S, the ordering of the C_{3v} rovibrational species would be A_1,E,E,A_2 at equally spaced energies $-S$, $-0.5S$, $0.5S$, and S, respectively, relative to the semiclassical rotational energy as shown in Fig. 7(a) and the right hand portion of Fig. 7(b). For certain values of the tunneling the superfine structure may resemble the form sketched on the left-hand side of Fig. 7(b).

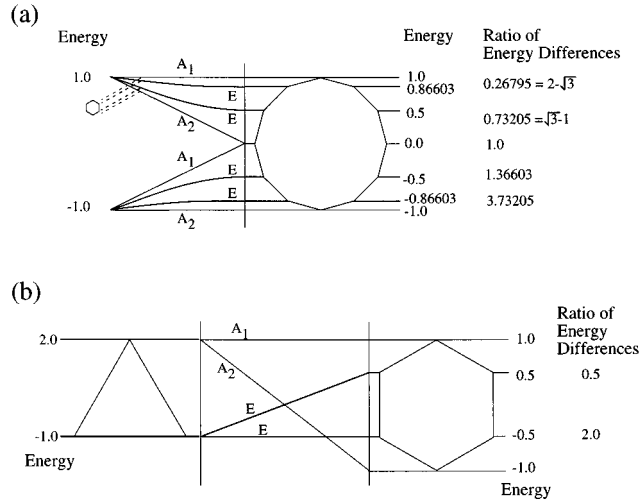

FIG. 7. Superfine structure of the subclusters $D_{3d}-C_{3v}$ symmetry breaking. (a) 12-fold clusters found near C_3 axes. (b) Sixfold clusters found near C_5 axes.

IX. CONCLUSION

The rotational level fine structure of symmetry-broken isotopomers of the 60 carbon fullerene including $^{13}C\ ^{12}C_{59}$ has been modeled along with other symmetry-breaking examples using semiclassical rotational energy surface analysis and related to exact quantum-mechanical energy eigenvalues. $^{13}C\ ^{12}C_{59}$ could be the major contributor to fine structure in a high resolution infrared scan of C_{60} produced using naturally occurring carbon. Such a spectrum would involve transitions between rovibrational states described herein and rotationally similar dipole active excited states. The added complexity of the states and levels owes to the nearly complete breaking of the icosahedral symmetry of $^{12}C_{60}$, the superposition of a slightly prolate symmetric rotor and the corresponding lifting of the strict bosonic exchange exclusion.

Nevertheless, the majority of the levels, particularly for higher J, show an ordering and sparseness characteristic of much higher symmetry rotors, and an improved physical understanding of the resulting rotational eigenstates is possible using semiclassical rotational energy surface analysis. The spectral sparseness is due to level clustering which in turn is due to multiple identical semiclassical trajectories that persist even for low symmetry rotor Hamiltonians.

ACKNOWLEDGMENTS

We would like to thank the Theoretical and Computational Chemistry division of the National Science Foundation for support on grant CHM 9221371. One of us (W.G.H.) would also like to thank the Institute for Theoretical Atomic and Molecular Physics (ITAMP) at the Harvard Smithsonian Center for Astrophysics for support during this period.

[1] W. Kratschmer *et al.*, Nature (London) **347**, 354 (1990).
[2] D. S. Bethune *et al.*, Chem. Phys. Lett. **174**, 219 (1990).
[3] S. Mayuma, L. R. Anderson, and R. E. Smalley, Rev. Sci. Instrum. **61**, 3686 (1990).
[4] S. Iijima, Nature (London) **354**, 56–58 (1991).

This article is copyrighted as indicated in the article. Reuse of AIP content is subject to the terms at: http://scitation.aip.org/termsconditions. Downloaded to IP: 132.248.9.8
On: Mon, 22 Dec 2014 16:28:40

[5] B. Guo, K. Kerns, and A. Castleman, Science **255**, 1411 (1992).
[6] J. R. Heath *et al.*, J. Am. Chem. Soc. **107**, 7779 (1985).
[7] T. Weiske *et al.*, Angew. Chem. Int. Ed. Engl. **30**, 884 (1991).
[8] M. M. Ross and J. R. Callahan, J. Phys. Chem. **95**, 5720 (1991).
[9] C. C. Henderson and P. A. Cahill, Science **259**, 1885 (1993).
[10] W. G. Harter and D. E. Weeks, Chem. Phys. Lett. **132**, 387 (1986).
[11] W. G. Harter, Comp. Phys. Reports **8** (6), 321 (1988).
[12] W. G. Harter and D. E. Weeks, J. Chem. Phys. **90**, 4727 (1989).
[13] W. G. Harter and T. C. Reimer, Chem. Phys. Lett. **194**, 230 (1992).
[14] W. G. Harter, *Principles of Symmetry, Dynamics and Spectroscopy* (Wiley, New York, 1993), pp. 124 and 199.
[15] D. E. Weeks and W. G. Harter, J. Chem. Phys. **90**, 4744 (1989).
[16] W. G. Harter and T. C. Reimer, J. Chem. Phys. **94**, 5426 (1991).
[17] D. E. Weeks and W. G. Harter, Chem. Phys. Lett. **176**, 209 (1991).
[18] C. I. Frum *et al.*, Chem. Phys. Lett. **176**, 504 (1991).
[19] D. E. Weeks, J. Chem. Phys. **96**, 7380 (1992).

This article is copyrighted as indicated in the article. Reuse of AIP content is subject to the terms at: http://scitation.aip.org/termsconditions. Downloaded to IP: 132.248.9.8
On: Mon, 22 Dec 2014 16:28:40